5

Gold Catalysts Supported on Nanostructured Materials: Support Effects

Wenfu Yan, Steven H. Overbury, and Sheng Dai*

5.1. INTRODUCTION

Although gold in bulk has often been regarded as poorly active as a catalyst, Haruta *et al*. found in the late 1980s and the early of 1990s that the gold particles deposited on selected metal oxides exhibit surprisingly high catalytic activity for CO oxidation at low temperature.[1,2] Now, an extensive body of literature describing the CO oxidation ability of gold nanoparticles supported on various metal oxides, such as TiO_2,[3–15] Fe_2O_3,[1,16] CO_3O_4,[1] NiO,[1] SiO_2,[17] ZrO_2,[18,19] and Al_2O_3,[20] has appeared.[21–30] The catalytic activities of gold catalysts depend on many factors. Among them, the variation in the properties of support oxides gives rise to much of the variability in supported gold catalysts, for example the effect of isoelectronic point (IEP) upon deposition of gold species or the role of the oxide reducibility in effecting the transfer of oxygen between the support and the gold nanoparticles. The focus of this chapter is the review of our recent research on the synthesis and characterization of tailored nanostructured supports for the assembly of ultrasmall gold nanoparticles for catalysis applications.

This chapter is divided into three parts. Firstly, the catalytic activities and stabilities of gold nanoparticles supported on allotropic TiO_2 phases are compared.[4] To understand the mechanism of catalysis of the gold nanoparticles deposited on metal

Chemical Sciences Division, Oak Ridge National Laboratory, Oak Ridge, TN 37831-6201
* To whom correspondence should be addressed. E-mail: dais@ornl.gov

oxides, it is of interest to study the effects of variability of support structures for a single type of oxide. Titania (TiO_2) is a good candidate for such investigation because of the existence of two main allotropic metastable forms: anatase and brookite. Secondly, a surface sol–gel (SSG) method for tailoring mesoporous silica materials for gold catalysis applications is reviewed.[15] The essence of this method is to change the surface IEPs of mesoporous silica through a monolayer surface functionalization with high-IEP oxides (e.g., TiO_2) for the assembly of ultrasmall gold inside mesopores. Thirdly, a building-block approach based on a layer-by-layer SSG process is discussed.[31] Fumed silica materials were modified with a stepwise SSG process for controlled growth of double layers consisting of TiO_2 and Al_2O_3 monolayers with different combinations on silica surfaces. The significant differences in activity of the gold catalysts supported on the silica supports with the different combinations of surface monolayers were observed.

5.2. EXPERIMENTAL SECTION

5.2.1. Preparation of Gold Nanocatalysts Supported on Anatase and Brookite

5.2.1.1. Sonication Synthesis of Anatase.[32] The detailed synthesis protocol has been given previously.[4] Briefly, 100 mL of deionized water was sonicated by employing a direct-immersion titanium horn (Sonics and Materials, VCX-750, 20 kHz, and starting power 100 W/cm^2) followed by the injection of 10 mL of tetraisopropyltitanate (Aldrich) into the sonication cell (glass beaker). The mixture was further sonicated continuously for 1 h. The sonication was conducted without cooling. The white precipitates were separated by centrifugation and washed three times with deionized water and once with ethanol. The product was dried in a desiccater overnight and was ground into a fine powder before the deposition of gold precursor.

5.2.1.2. Hydrothermal Synthesis of Brookite.[33] Typically, NaOH solution (2 M) was added to 5 mL titanium tetrachloride with stirring to adjust the pH value of the solution to 10, producing a basic colloidal solution. The solution obtained was transferred into an autoclave and heated at 200°C for 24 h. The white precipitates were separated by centrifugation and washed three times with deionized water and once with ethanol. The product was dried at 70°C in air overnight and was ground to a fine powder before the deposition of gold precursor on its surface.

5.2.1.3. Deposition–Precipitation (DP) of Gold Precursor Species on Anatase and Brookite. First, weighed amounts of hydrogen tetrachloroaurate(III) trihydrate ($HAuCl_4 \cdot 3H_2O$, 99.9+%, Aldrich) were dissolved into 50 mL deionized water, a process that depends on the gold loading in the gold catalyst. The pH value of the resulting solution was adjusted to 10.0 with vigorous stirring, using a solution of 1.0 M KOH at room temperature to displace Cl^- with hydroxyl on the gold precursor.[34] After pH adjustment, the solution was heated in an 80°C water bath followed by the addition of 1.0 g of TiO_2 powder. The resulting mixture was continually stirred for 2 h to permit the gold precursor to react with and displace surface hydroxyls. Finally, the precipitates were separated by centrifugation and washed three times with deionized water and

once with ethanol to remove Cl^-. The product was dried at 40°C temperature in air overnight to obtain the "as-synthesized" catalyst.

5.2.2. Preparation of Gold Nanocatalysts Supported on Mesoporous Silica Modified with Oxide Monolayer

5.2.2.1. Surface Sol–Gel Modification of Mesoporous Silica Materials with TiO_2 Monolayer.[15] The mesoporous material used in this investigation is SBA-15. The SBA-15 silica was prepared using Pluronic P123 (Aldrich) and tetraethylorthosilicate (TEOS, Aldrich) according to the procedure described in the literature.[35] The procedure used for the preparation of one-layer or multilayer titanium oxide on SBA-15 powders was developed according to the method described by Kunitake and coworkers[36] for the preparation of ultrathin films of metal oxides on hydrolyzed surfaces. The homemade apparatus for conducting the surface sol–gel process on the mesopore surfaces of powdered materials consists of two parts: an evacuation system and a fritted reactor. Typically, 1.0 g of pre-dried SBA-15 powder was loaded into the fritted reactor, which was sealed with a rubber septum at one end and connected to a vacuum system at the other end. The initially loaded sample was evacuated at ambient temperature and purged by nitrogen. This cycle was repeated several times. Subsequently, the stop-cock separating the vacuum system and the reactor was closed and 5 mL of titanium(IV) butoxide (Aldrich, 97%) in the mixture of 10 mL anhydrous toluene (Aldrich, 99.8%) and 10 mL anhydrous methanol (Aldrich, 99.8%) was transferred into the reactor through a syringe. After 30 min reaction, the solution was completely removed via vacuum filtration. Anhydrous methanol (5 mL) was injected into the reactor to wash off the unreacted titanium(IV) butoxide. The resulting sample was dried via vacuum evacuation. An excess amount of deionized water was then injected into the glass tube to hydrolyze the monolayer of titanium oxide. The final product can be washed thoroughly with anhydrous methanol and dried for the coating of the second layer. The multilayers of titanium oxide on SBA-15 can be prepared by iteration of the above procedure.

5.2.2.2. Assembly of Ultrasmall Gold Nanoparticles on Surface-Modified Mesoporous Silica. Firstly, 3.0 g of hydrogen tetrachloroaurate(III) trihydrate ($HAuCl_4 \cdot 3H_2O$, 99.9+%, Aldrich) was dissolved into 500 mL deionized water to form the gold precursor solution. Typically, the pH value of the pre-weighed gold precursor solution (20 mL) was adjusted to about 10 with vigorous stirring using a solution of 1.0 M KOH at room temperature. The solution was then heated via an 80°C water bath, and a surface-modified SBA-15 (0.4 g) without any pretreatment was added with stirring. The resulting cloudy solution was continually stirred for 2 h. The precipitates were separated by centrifugation and washed three times with deionized water. The yellow product was dried at 40°C overnight.

5.2.3. Preparation of Gold Nanocatalysts Supported on Silica Modified with Oxide Double Layers

5.2.3.1. Surface Sol–Gel Modification of Fumed Silica with TiO_2/Al_2O_3 or Al_2O_3/TiO_2 Double Layer. The basic procedure for functionalization of Cab-O-Sil silica

surfaces with the double layers of TiO_2 and Al_2O_3 was the same as that given in Section 5.2.2.1. Typically, a pre-weighed SiO_2 powder sample (9.8 g) was loaded into a reflux bottle and dried at 125°C for 16 h. The bottle was then sealed with a pre-dried rubber septum. Subsequently, the metal oxide precursor [7.9 g $Ti(OBu^n)_4$ for titania or 7.7 g $Al(OBu^s)_3$ for alumina] and the anhydrous mixture of toluene (100 mL) and methanol (100 mL) were transferred into the bottle through a syringe. The resulting solution was refluxed for 3 h. The final product was filtered, washed several times with anhydrous ethanol, hydrolyzed with deionized water, and dried at 80°C overnight. The iteration of the above sequential condensation and hydrolysis reactions allows the coating of the second monolayer on the one generated in the previous deposition cycle. For comparison, we have also synthesized Cab-O-Sil silica functionalized with TiO_2 or Al_2O_3 monolayer.

5.2.3.2. Deposition–Precipitation (DP) of Gold Precursor on Surface-Modified Amorphous Silica. The gold nanoparticles were deposited on the above surface-modified amorphous silicas by using the same process as that given in Section 5.2.2.2.

5.2.4. Measurements of Catalytic Performance for CO Oxidation

The CO oxidation reaction was carried out in a plug-flow microreactor (AMI 200, Altamira Instruments). Typically, 50 mg of catalyst was packed into a 4-mm-ID quartz U-tube, supported by quartz wool. Sample treatments were carried out on the same instrument, using either 8% O_2/He for oxidations or 12% H_2 mixed with Ar for reductions. For each treatment, gas flow was initiated near room temperature. The temperature was then ramped at 10°C/min to the target, held for 30 min, and then cooled to reaction temperature in the gas. Each pretreatment was followed by activity measurements made as follows. A gas stream of 1% CO balanced with dry air (<4 ppm water) was flowed at ambient pressure through the catalyst at a rate that was adjusted from sample to sample to maintain a constant space velocity of 44,400 mL/($h \cdot g_{cat.}$), or about 37 cm^3/min. Gas exiting the reactor was analyzed via a Buck Scientific 910 gas chromatograph equipped with a dual molecular sieve/porous polymer column (Alltech CTR1) and using a thermal conductivity detector. Typically, the sample was cooled to low temperature and the exiting gas was analyzed at regular intervals as the sample was slowly warmed. The reaction temperature was varied using an oven or by immersing the U-tube in a Dewar of ice water or cooled acetone, which slowly warmed (typically 0.1 to 0.2°C/min) throughout a period of approximately 10 h. The resulting curve of conversion vs. temperature was used to assess the activity after each treatment.

5.2.5. Characterization Methods

Powder X-ray diffraction (XRD) data were collected via a Siemens D5005 diffractometer with CuKα radiation ($\lambda = 1.5418$ Å). Routine transmission electron microscopy (TEM) and Z-contrast microscopy were carried out using an HITACH HD-2000 scanning transmission electron microscope (STEM) operated at 200 kV. Nitrogen gas adsorption measurements (Micromeritics Gemini) were used to determine the surface area and porosity of the catalyst supports. Inductively coupled plasma (ICP) analysis was performed via an IRIS Intrepid II XSP spectrometer (Thermo Electron Corporation).

5.3. RESULTS AND DISCUSSION

5.3.1. Support Effects from Structural Differences of the TiO_2 Allotropes (Anatase and Brookite)

Previously published work has demonstrated that the photocatalytic efficiency of titania depends upon its crystalline form. This variability has been attributed to differences in the rates of recombination, adsorptive affinity, or band gap between the rutile and anatase phases of titania.[37–39] In titania containing mixed phases of rutile and anatase, such as Degussa P25, enhanced activity for photocatalytic oxidation may also depend on crystallite morphology and interfacial contact.[39] It is therefore of interest to understand how differences in the structure of a titania support may affect other oxidative catalytic processes in gold catalysts. It has been shown that the selectivity in propylene epoxidation is improved by using anatase rather than rutile for catalysts prepared by DP of gold.[40] Higher activity for CO oxidation is observed for anatase compared with rutile when gold is deposited via a rather unconventional ion-cluster beam deposition approach.[41] The contacts at the Au-TiO_2 interfaces are also believed to play an important role in CO oxidation.[42]

Both anatase and brookite are metastable phases that can be readily converted to rutile upon heating at temperatures above 700°C.[43] In both metastable phases, the coordination of titanium is sixfold, with oxygen anions forming a distorted octahedron, and the oxygen atom being shared by three adjacent titanium atoms. However, the different stacking sequences and distortions of the Ti-O octahedral units in these two phases lead to crystallographic differences, thereby resulting in the different arrangement of the Ti–O and Ti–OH bonds on the surface of the corresponding nanoparticles. The structure of the most stable surfaces of anatase has been examined.[44] The (101) surface of anatase exhibits twofold coordinate oxygen anions and fivefold titanium cations, with the oxygen anions being more widely spaced on the anatase surface than on the brookite. The different spacing and symmetry of these Ti–O and –OH bonds on the surface of anatase and brookite can affect the deposition of the gold hydroxyl precursor on the surface of titania particles during the DP process. The systematic study of catalytic reactions on anatase-and brookite-supported gold catalysts can provide new insight into the catalytic mechanism of the gold nanoparticles deposited on metal oxides.

Nanosized anatase ($\leq$10 nm) and brookite ($\sim$70 nm) particles have been successfully synthesized via sonication and hydrothermal methods. Figure 5.1 shows the powder XRD patterns of as-synthesized anatase and brookite nanoparticles. The particle sizes were characterized by XRD and scanning electron microscopy (SEM) (Fig. 5.2).

Gold precursor was deposited on the surface of the nanosized particles of as-synthesized anatase and brookite supports via a DP process. The XRD patterns of the resulting samples (Fig. 5.1) show no metallic gold peaks, indicating that no redox reactions occur during the DP process or that the metallic gold particles are not large enough to generate observable XRD peaks.

Curves (a) and (b) in Fig. 5.3 compare the light-off curves for the gold catalysts supported on anatase and brookite after being treated with O_2 at 300°C. Interestingly, the catalytic activity of the brookite-supported gold catalyst remained highly active, with the onset for 100% CO conversion occurring around -20°C. In contrast, the onset

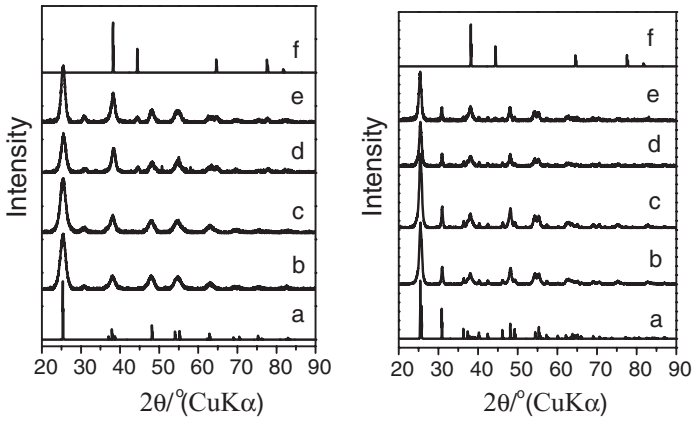

FIGURE 5.1. *Left*: Powder XRD patterns of (a) anatase simulated, (b) anatase as-synthesized, (c) as-synthesized Au-anatase, (d) Au-anatase treated at 300°C in O_2, (e) Au-anatase treated at 500°C in O_2, and (f) Au simulated. *Right*: Powder XRD patterns of (a) brookite simulated, (b) brookite as-synthesized, (c) as-synthesized Au-brookite, (d) Au-brookite treated at 300°C in O_2, (e) Au-brookite treated 500°C in O_2, and (f) Au simulated.

for 100% conversion of CO was obtained at 60°C for the anatase-supported catalyst treated under the same conditions.

The XRD patterns of both catalysts after treatment with O_2 at 300°C are compared in Fig. 5.1 (curves d). Clearly, the Au-anatase catalyst exhibits gold XRD peaks, indicating the formation of large metallic gold nanoparticles (diameter >20 Å) on the anatase support. The XRD pattern of the corresponding brookite-supported catalyst gives no XRD peaks associated with the large metallic gold nanoparticles.

The light-off curves of CO oxidation over Au-anatase and Au-brookite catalysts after treatment at 500°C in O_2 are shown in curves (c) and (d), respectively, in Fig. 5.3. Both catalysts were deactivated by this heat treatment; however, the Au-brookite remains significantly more active than the Au-anatase. The onset of 100% CO conversion for the Au-brookite occurs at approximately 60°C, while the corresponding onset for the Au-anatase occurs at temperatures as high as 160°C. The corresponding XRD patterns of these two samples are shown in Fig. 5.1 [curves (e)]. A very weak gold XRD peak at $2\theta \approx 44.5^\circ$ can be seen in the XRD pattern of Au-brookite treated at 500°C in

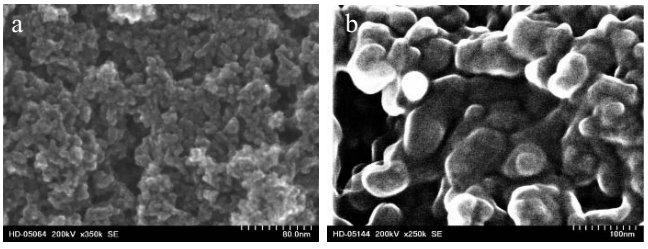

FIGURE 5.2. SEM images of as-synthesized (a) anatase and (b) brookite.

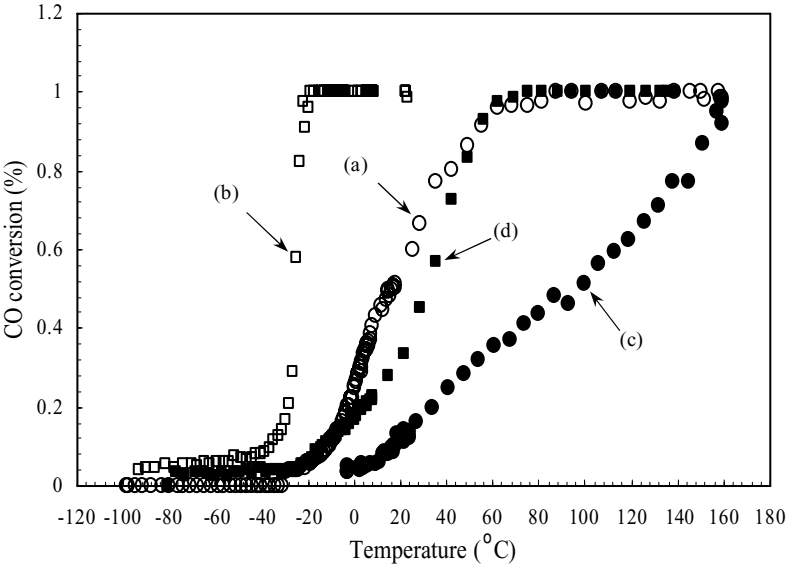

FIGURE 5.3. CO conversion vs. reaction temperature over supported gold catalysts: (a) Au-anatase treated at 300°C in O_2, (b) Au-brookite treated at 300°C in O_2, (c) Au-anatase treated at 500°C in O_2, and (d) Au-brookite treated at 500°C in O_2.

O_2, which indicates the formation via sintering of a small population of gold nanoparticles >3 nm. The gold XRD peaks for Au-anatase after treatment with O_2 at 500°C are more intense than those occurring after treatment with O_2 at 300°C, which indicates a significant increase in the population of large gold nanoparticles (>3 nm). Accordingly, the brookite-supported gold nanoparticles are significantly more stable against the temperature-induced aggregation than the anatase-supported gold nanoparticles.

This assertion about the stability of gold nanoparticles against aggregation on brookite surfaces is also consistent with the microscopy investigation performed using an HD-2000 STEM (probe size $\approx$ 0.3 nm) operating at 200 kV. Dark-field imaging with a high-angle annular dark-field (HAA-DF) detector provides higher contrast for small clusters of heavy elements in a low-atomic-number matrix as compared with conventional TEM. The nature of gold nanoparticles deposited on anatase and brookite makes these samples well suited to HAA-DF (also known as Z-contrast) STEM imaging. Figure 5.4 shows the comparison of the dark-field STEM images of the gold catalysts supported on anatase and brookite after treatment with O_2 at 300°C followed by treatment at 500°C. As seen in Fig. 5.4, the concentration of the large gold particles (>3 nm) on brookite is lower than that occurring on anatase. However, there is a significant population of small particles (<2 nm) retained on brookite. Thermally induced growth of particles observed in XRD and STEM was further confirmed by X-ray extended absorption spectroscopy, which also clearly indicated that gold supported on anatase sinters more facilely than on brookite.[45] Therefore, the loss of catalytic activity of the gold nanoparticles supported on anatase can be correlated to the higher tendency for the small gold nanoparticles to sinter on anatase during high-temperature O_2 treatment.

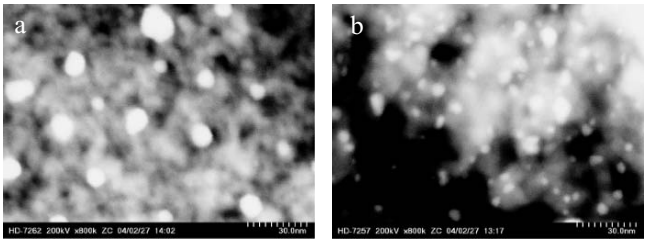

FIGURE 5.4. Dark-field STEM images of the gold catalysts after being treated at 500°C in O_2: (a) Au-anatase and (b) Au-brookite.

Further support for the assertion that gold nanoparticles are more susceptible to sintering on anatase than on brookite comes from the analysis of surface areas and gold loadings. The surface area of as-synthesized anatase is 225 m^2/g, while it is only 106 m^2/g for the as-synthesized brookite. The gold loadings of Au-anatase and Au-brookite determined via inductively coupled plasma-atomic emission (ICP-AE) are 2.8 wt.% and 3.2 wt.%, respectively. Since the surface density of gold is lower on anatase, this catalyst might be expected to be more stable against sintering than for Au on the brookite, if the surface properties of anatase and brookite, as well as the interaction between gold nanoparticles and support, are similar. This is clearly opposite to the above experimental observation. The difference of the sintering tendency of the gold nanoparticles dispersed on the surface of anatase and brookite must come from the different surface properties of these supports. A stronger interaction between gold nanoparticles and brookite surface or a higher barrier for particle coarsening might exist to slow down the kinetics for movement or thickening of the small gold nanoparticles.[46]

In conclusion, the stability of gold nanoparticles against sintering on brookite and anatase is very different. A highly stable catalytic system for CO oxidation based on the brookite-supported gold catalyst has been developed. The high stability of Au-brookite could result from the unique surface property of brookite. The interaction between gold nanoparticles and support plays the important role of stabilizing the catalyst in high-temperature environments. Work is currently under way to explore the applications of the Au-brookite catalyst in other catalytic processes.

5.3.2. Support Effects from Surface-Modified Mesostructured Substrates

The key effect of oxide supports on the catalytic activities of metal particles is exerted through the interface between oxides and metal particles. The key objective of this study is to develop synthesis methodologies for tailoring this interface. Here, an SSG approach was introduced to modify the surface of mesoporous silica materials with ultrathin films of titanium oxide so that the uniform deposition of gold precursors on ordered mesoporous silica materials by DP could be achieved without the constraint of the low IEP of silica. The surface sol–gel process was originally developed by Kunitake and coworkers.[36,47–49] This novel technology enables molecular-scale control of film thickness over a large 2-D substrate area and can be viewed as a solution-based

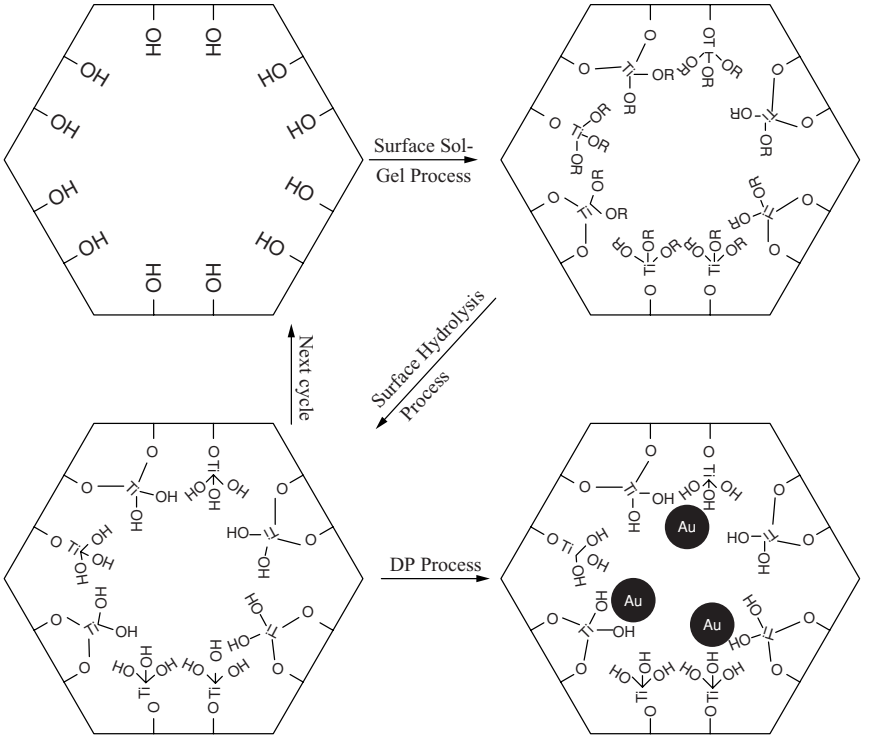

SCHEME 5.1.

methodology for atomic layer deposition (ALD) synthesis.[50–52] The surface sol–gel technique generally consists of two-half reactions: (1) nonaqueous condensation of metal-alkoxide precursor molecules with surface hydroxyl groups and (2) aqueous hydrolysis of the adsorbed metal-alkoxide species to regenerate surface hydroxyls. Iteration of the above sequential condensation and hydrolysis reactions allows the layer-by-layer coating of a selected metal oxide on a hydroxyl-terminated surface. Scheme 5.1 is a schematic diagram of the basic synthesis protocol for ultrathin TiO_2 on SBA-15. The SBA-15 materials have hexagonally packed channels with pore sizes of ~7.4 nm. The large mesopores allow a facile transport of metal-alkoxide reactants inside the mesopores not only for monolayer but also for multilayer functionalization on the internal walls of SBA-15.

Figure 5.5 shows the variation of the pore size distribution as a function of cycles of surface-modification-based N_2 adsorption isotherms. The pore size decreases with the modification cycle number. The reduction of the mesopore size for each cycle should be about twice the single-layer thickness. Accordingly, the effective single-layer thickness is about 6 to 7 Å based on the above BET measurements. This value is close to those estimated from the frequency changes of a quartz crystal balance for ultrathin films prepared by the surface sol–gel process on 2-D substrates.[47–49]

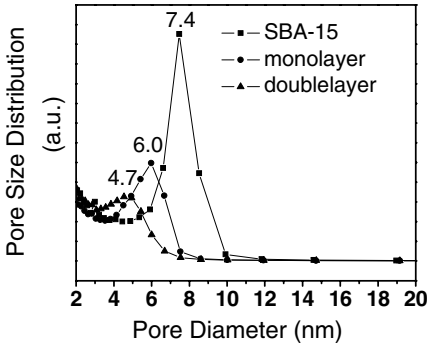

FIGURE 5.5. Pore size distributions as a function of the number of TiO_2 layers.

Another consequence of this surface sol–gel process on SBA-15 is the reduction of the surface silanol groups induced by the condensation reaction with titanium butoxide. The reaction, after hydrolysis, converts surface silanol functionality, $(SiO)_3SiOH$, into Ti-OH functionality. Given the similar electronegativity of silicon (1.8) and titanium (1.7), the expected consequence of this modification in the solid state ^{29}Si NMR is a decrease in the Q^3 band and a corresponding increase in the Q^4 band; that is, the $OTi(OH)_3$ and $OSi(OH)_3$ ligands will cause equivalent NMR shift perturbations on the substituted silicon site.

The solid-state ^{29}Si SPE NMR spectra of SBA-15 and the titania surface-coated SBA-15 (Ti-SBA-15) are in accord with this expectation. The spectrum of SBA-15 displays a broad asymmetric peak at 109 ppm (Q^4 sites) with shoulders at -101 ppm (Q^3 sites) and 90 ppm (Q^2 sites) in the area ratio 79:19:2. The NMR spectrum of Ti-SBA-15 (one layer) shows a reduction of the Q^3 band intensity relative to the Q^4 intensity. The normalized Q^4:Q^3:Q^2 site populations become 85:13:2. No asymmetry is observed in the Q^4 site band. Repetition of the monolayer deposition to form a double layer of titania on silica yields a material whose ^{29}Si NMR spectrum is indistinguishable from that of the Ti-SBA-15 with a monolayer coverage. As expected, the titania-insulated silica resonances are unperturbed by the second titania layer.

The gold precursors were readily introduced via the DP method on the surfaces of the modified mesoporous materials. The subsequent reduction of the surface-immobilized gold precursors with CO successfully led to gold nanoparticles assembled inside ordered mesopores. Figure 5.6 shows the Z-contrast TEM image of the resulting materials. The tiny, highly uniform bright spots (0.8 to 1.0 nm diameter) along the mesopore channels in Fig. 5.6 correspond to the gold nanoparticles. The Z-contrast TEM imaging provides direct proof of the presence of the metallic gold nanoparticles within the channels of SBA-15. The key point with HAA-DF imaging is that the intensity of the Rutherford scattered beams is directly proportional to Z^2, where Z is the atomic number of the scattering element. Thus, heavy atoms (such as gold) stand out very clearly on a light background of silicon and oxygen. The energy-dispersive X-ray (EDX) spectroscopy analysis of the composition of this range in Fig. 5.6 is in agreement with the presence of gold and titanium. The preparation of gold nanoparticles on SBA-15 (without titania monolayer) by the DP method resulted in only a

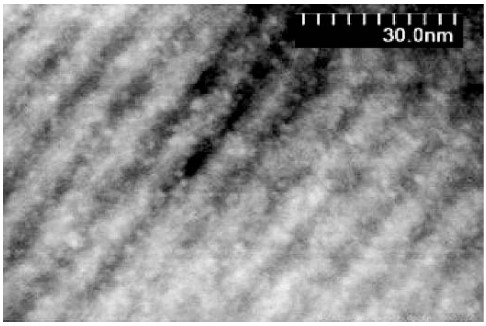

FIGURE 5.6. Z-contrast TEM image of ultrasmall gold nanoparticles on ordered mesoporous materials. The bright spots (0.8∼1.0 nm) correspond to gold nanoparticles.

small population of very large gold nanoparticles aggregated on the external surfaces of SBA-15. This observation clearly demonstrated the importance of TiO_2 surfaces for the immobilization and the stabilization of gold nanoparticles.

The activity of the gold catalysts for CO oxidation was characterized via a plug-flow reactor using 1% CO/dry air at a space velocity at 44,400 $cm^3/(g_{cat} \cdot h)$. Comparisons were made between the Au/monolayer TiO_2-SBA-15 and the Au/commercial nanocrystalline titania support (Degussa P25). Comparably high activities (i.e., achieving 50% CO conversion above about $-40^\circ C$) were found for the as-synthesized gold catalysts. High-temperature (300°C, 30 min) 8%O_2/He treatment dramatically decreased the activity of nanocrystalline TiO_2-supported catalysts, as the light-off curve shifted to high temperature. This deactivation can be attributed primarily to the aggregation of gold nanoparticles.[24] By contrast, the activity of the monolayer catalyst did not change significantly, achieving >50% conversion at $-25^\circ C$.

5.3.3. Support Effects from the Different Combinations of Oxide Monolayers Sequentially Coated on the Surface of Amorphous Silica

As discussed in the above section, the self-limiting nature of the SSG process is key to the success of the layer-by-layer functionalization. The SSG process is a versatile technique that can be utilized for the functionalization of oxide supports with both single and multiple oxide components. The objective of the current study is to generate more complex multicomponent oxide surfaces via the SSG process for the investigation of the support effects in gold catalysis. The surfaces discussed here consist of two sequential combinations of TiO_2 and Al_2O_3 monolayers on amorphous silica: (1) $Al_2O_3/TiO_2/SiO_2$ (SiO_2 coated with the first layer of TiO_2 and the second layer of Al_2O_3) and (2) $TiO_2/Al_2O_3/SiO_2$ (SiO_2 coated with the first layer of Al_2O_3 and the second layer of TiO_2). For comparison, we have also prepared the same silica sample functionalized by TiO_2 (TiO_2/SiO_2) or Al_2O_3 (Al_2O_3/SiO_2) monolayers.

XRD analyses revealed the amorphous nature of the mono/multilayers of TiO_2 and/or Al_2O_3 on fumed silica. Elemental analyses of the samples of $Au/TiO_2/SiO_2$, $Au/Al_2O_3/SiO_2$, $Au/Al_2O_3/TiO_2/SiO_2$, and $Au/TiO_2/Al_2O_3/SiO_2$ showed that the gold weight loadings for these four samples were 5.1, 7.9, 10.3, and 11.7%, respectively.

Figure 5.7 shows the light-off curves of $Au/TiO_2/SiO_2$, $Au/Al_2O_3/SiO_2$, $Au/Al_2O_3/TiO_2/SiO_2$, and $Au/TiO_2/Al_2O_3/SiO_2$. These light-off curves were measured from the samples both as-synthesized and pretreated under the following conditions: 150°C in H_2 (50% H_2/He) and 150°C in O_2 (8% O_2/He).

The gold nanoparticles deposited on the surface of unmodified fumed silica with the DP method show no activity for CO oxidation (not shown). No clear improvement of the catalytic activities was observed for the gold nanoparticles on SiO_2 whose surface was modified with an Al_2O_3 monolayer through the SSG process. The as-synthesized $Au/Al_2O_3/SiO_2$ sample had a very low conversion at high temperature but was quickly deactivated. The initial low activity can be attributed to the reduction of cationic gold species to metallic gold by CO, which disappeared after the cationic gold species were totally consumed. This conjecture is also consistent with the observations that the catalysts pretreated at 150°C (either in H_2 and in O_2) exhibit no activities.

The further surface modification of Al_2O_3-modified fumed silica with a TiO_2 monolayer resulted in a double-layer-coated support ($TiO_2/Al_2O_3/SiO_2$). The deposition of gold nanoparticles on this double-layer-coated support ($Au/TiO_2/Al_2O_3/SiO_2$) via DP gave rise to a highly active catalyst for CO oxidation. For the as-synthesized catalyst, a 50% conversion was observed at −22°C (specific rate: 0.085 $mol_{CO}/g_{Au}/h$). The treatment at 150°C (either in O_2 or H_2) slightly decreased its activity. The catalysts treated at 150°C in O_2 and H_2 have 50% conversion temperatures at about −18°C and −11°C (specific rate: 0.085 $mol_{CO}/g_{Au}/h$), respectively.

In contrast to the Al_2O_3-modified fumed silica (Al_2O_3/SiO_2), the TiO_2-modified fumed silica (TiO_2/SiO_2) is a good substrate for the preparation of highly active gold nanocatalysts. The gold nanoparticles deposited on TiO_2/SiO_2 exhibited a high activity for low-temperature CO oxidation. For the as-synthesized catalyst, the 50% conversion temperature (specific rate: 0.194 $mol_{CO}/g_{Au}/h$) is as low as −44°C, which is much lower than that of $Au/TiO_2/Al_2O_3/SiO_2$. The reduction at 150°C in H_2 decreased the activity, giving rise to a 50% conversion temperature at −32°C. Surprisingly, the treatment at the same temperature in O_2 increased the activity of this catalyst, with a 50% conversion temperature approaching −54°C. The enhanced activity could be attributed to the surface restructuring of cationic gold species on the TiO_2 monolayer to enhance the interaction at the interface.

The further surface modification of the TiO_2-modified fumed silica with an Al_2O_3 monolayer gave rise to another double-layer-coated support ($Al_2O_3/TiO_2/SiO_2$) whose monolayer functionalization sequence is the reverse of $TiO_2/Al_2O_3/SiO_2$. A new gold nanocatalyst ($Au/Al_2O_3/TiO_2/SiO_2$) was prepared through DP of gold precursors on the surface of $Al_2O_3/TiO_2/SiO_2$. The as-synthesized gold nanocatalyst gave a 50% conversion temperature (specific rate: 0.096 $mol_{CO}/g_{Au}/h$) at −31°C, which is more active than that for $Au/TiO_2/Al_2O_3/SiO_2$ but less active than that for $Au/TiO_2/SiO_2$. The treatment at 150°C in O_2 just slightly increased the activity of $Au/Al_2O_3/TiO_2/SiO_2$, unlike the significant increase in the case of $Au/TiO_2/SiO_2$. However, the treatment at 150°C in H_2 considerably increased the activity of $Au/Al_2O_3/TiO_2/SiO_2$. The catalyst treated in H_2 at 150°C is highly active even at −94°C, with 75% conversion (specific rate: 0.144 $mol_{CO}/g_{Au}/h$). In sharp contrast, the $Au/TiO_2/SiO_2$ catalyst treated in H_2 at 150°C had only 17% conversion (specific rate: 0.066 $mol_{CO}/g_{Au}/h$) at this temperature.

In conclusion, the sequence of activities induced via surface layer structures for the as-synthesized form of these four gold nanocatalysts is: $Au/TiO_2/SiO_2 > Au/$

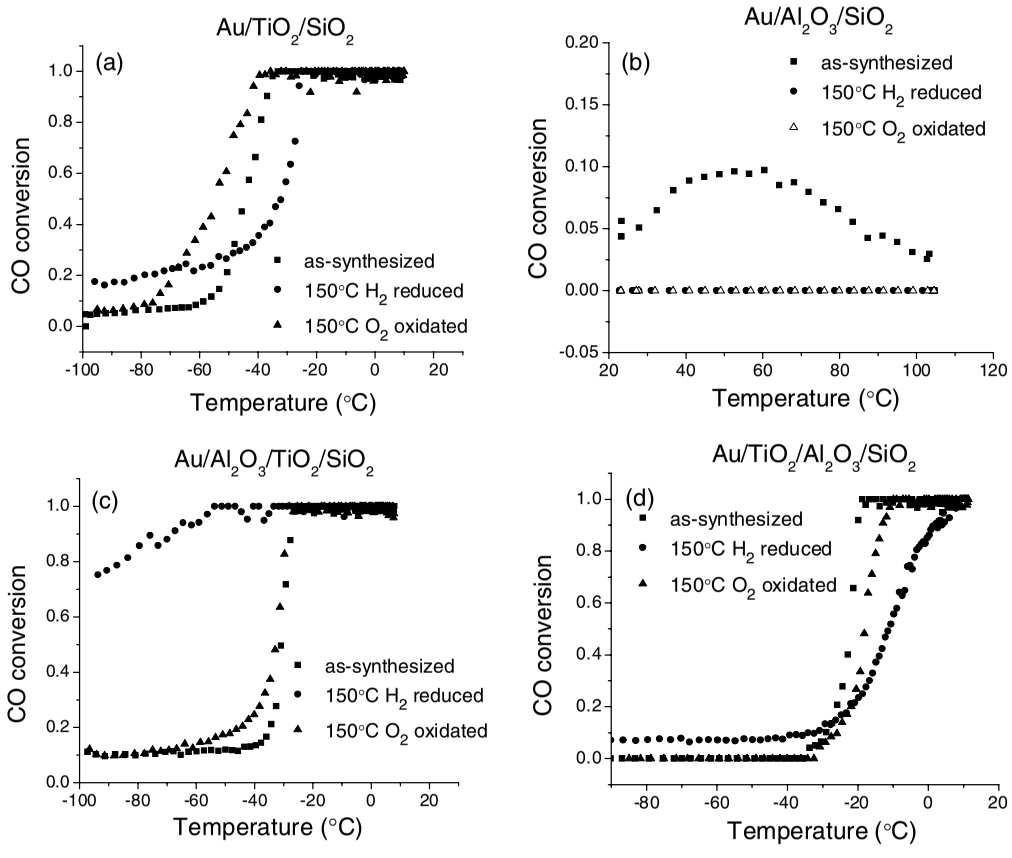

FIGURE 5.7. The light-off curves of as-synthesized $Au/TiO_2/SiO_2$, $Au/Al_2O_3/SiO_2$, $Au/Al_2O_3/TiO_2/SiO_2$, and $Au/TiO_2/Al_2O_3/SiO_2$ and the same samples under treatments of 150°C in H_2 (50% H_2/He) and 150°C in O_2 (8% O_2/He).

$Al_2O_3/TiO_2/SiO_2$ > $Au/TiO_2/Al_2O_3/SiO_2$ >> $Au/Al_2O_3/SiO_2$. However, the $Au/Al_2O_3/TiO_2/SiO_2$ catalyst treated in H_2 at 150°C is the most active in this series based on the layer-by-layer functionalization of silica. The functionalization sequence is an important factor in determining the catalytic activities of the resulting gold catalysts. The activity of $Au/TiO_2/SiO_2$ is higher than that of $Au/TiO_2/Al_2O_3/SiO_2$, indicating that the Al_2O_3 sublayer has a negative effect on the activity of the resulting catalyst. On the other hand, the activity of $Au/Al_2O_3/TiO_2/SiO_2$ is much higher than that of $Au/Al_2O_3/SiO_2$, implying that the TiO_2 sublayer has a positive effect on the resulting catalyst.

5.4. CONCLUSIONS

In summary, the studies on the activity and stability of the gold nanocatalysts supported by TiO_2 anatase and brookite nanoparticles indicate that the stability of gold nanoparticles against sintering on two catalysis systems is very different despite the same chemical composition. The high stability of the brookite-supported gold catalyst could result from the unique surface property of TiO_2 brookite. Another methodology discussed here for tailoring the surface properties of catalyst supports is the generation of amorphous TiO_2 monolayers on mesoporous silica materials. The high catalytic activity and stability of the gold nanoparticles deposited on the TiO_2-modified mesoporous silica surface for low-temperature CO oxidation indicate that the amorphous TiO_2 monolayer on the surface of silica is also a good support for gold catalysts. The significant activity differences among the gold nanocatalysts supported on TiO_2/SiO_2, Al_2O_3/SiO_2, $Al_2O_3/TiO_2/SiO_2$, and $TiO_2/Al_2O_3/SiO_2$ highlight a unique support effect that the sequence of the metal-oxide monolayers on silica surfaces has in determining the activities of supported gold nanocatalysts.

ACKNOWLEDGMENTS

This work was conducted at the Oak Ridge National Laboratory and supported by the Division of Chemical Sciences, Office of Basic Energy Sciences, U.S. Department of Energy, under contract No. DE-AC05-00OR22725 with UT-Battelle, LLC. This research was supported in part by an appointment for W.Y. to the Oak Ridge National Laboratory Postdoctoral Research Associates Program administered jointly by the Oak Ridge Institute for Science and Education and Oak Ridge National Laboratory. We gratefully acknowledge the help from Dr. Bei Chen for the catalytic test, Dr. Zongtao Zhang for the measurement involving SEM, Dr. Shannon M. Mahurin for analyses involving TEM and Z-contrast TEM, and Dr. Edward W. Hagaman for the NMR analysis.

REFERENCES

1. M. Haruta, N. Yamada, T. Kobayashi, and S. Iijima, Gold catalysts prepared by coprecipitation for low-temperature oxidation of hydrogen and of carbon-monoxide, *J. Catal.* **115**(2), 301–309 (1989).

2. M. Haruta, S. Tsubota, T. Kobayashi, H. Kageyama, M. J. Genet, and B. Delmon, Low-temperature oxidation of Co over gold supported on TiO_2, alpha-Fe_2O_3, and Co_3O_4, *J. Catal.* **144**(1), 175–192 (1993).
3. S. D. Lin, M. Bollinger, and M. A. Vannice, Low-temperature CO oxidation over Au/TiO_2 and Au/SiO_2 catalysts, *Catal. Lett.* **17**(3–4), 245–262 (1993).
4. W. F. Yan, B. Chen, S. M. Mahurin, S. Dai, and S. H. Overbury, Brookite-supported highly stable gold catalytic system for CO oxidation, *Chem. Commun.* 1918–1919 (2004).
5. Y. Z. Yuan, A. P. Kozlova, K. Asakura, H. L. Wan, K. Tsai, and Y. Iwasawa, Supported Au catalysts prepared from Au phosphine complexes and As-precipitated metal hydroxides: Characterization and low-temperature CO oxidation, *J. Catal.* **170**(1), 191–199 (1997).
6. J. D. Grunwaldt, C. Kiener, C. Wogerbauer, and A. Baiker, Preparation of supported gold catalysts for low-temperature CO oxidation via "size-controlled" gold colloids, *J. Catal.* **181**(2), 223–232 (1999).
7. G. R. Bamwenda, S. Tsubota, T. Nakamura, and M. Haruta, The influence of the preparation methods on the catalytic activity of platinum and gold supported on TiO_2 for CO oxidation, *Catal. Lett.* **44**(1–2), 83–87 (1997).
8. M. Okumura, K. Tanaka, A. Ueda, and M. Haruta, The reactivities of dimethylgold(III)beta-diketone on the surface of TiO_2—A novel preparation method for Au catalysts, *Solid State Ionics* **95**(1–2), 143–149 (1997).
9. M. A. P. Dekkers, M. J. Lippits, and B. E. Nieuwenhuys, CO adsorption and oxidation on Au/TiO_2, *Catal. Lett.* **56**(4), 195–197 (1998).
10. M. Valden, S. Pak, X. Lai, and D. W. Goodman, Structure sensitivity of CO oxidation over model Au/TiO_2 catalysts, *Catal. Lett.* **56**(1), 7–10 (1998).
11. M. Valden, X. Lai, and D. W. Goodman, Onset of catalytic activity of gold clusters on titania with the appearance of nonmetallic properties, *Science* **281**(5383), 1647–1650 (1998).
12. J. D. Grunwaldt, and A. Baiker, Gold/titania interfaces and their role in carbon monoxide oxidation, *J. Phys. Chem.* B **103**(6), 1002–1012 (1999).
13. G. Mul, A. Zwijnenburg, B. van der Linden, M. Makkee, and J. A. Moulijn, Stability and selectivity of Au/TiO_2 and $Au/TiO_2/SiO_2$ catalysts in propene epoxidation: An in situ FT-IR study, *J. Catal.* **201**(1), 128–137 (2001).
14. M. Date, Y. Ichihashi, T. Yamashita, A. Chiorino, F. Boccuzzi, and A. Haruta, Performance of Au/TiO_2 catalyst under ambient conditions, *Catal. Today* **72**(1–2), 89–94 (2002).
15. W. F. Yan, B. Chen, S. M. Mahurin, E. W. Hagaman, S. Dai, and S. H. Overbury, Surface sol-gel modification of mesoporous silica materials with TiO_2 for the assembly of ultrasmall gold nanoparticles, *J. Phys. Chem.* B **108**(9), 2793–2796 (2004).
16. F. Boccuzzi, A. Chiorino, M. Manzoli, D. Andreeva, and T. Tabakova, FTIR study of the low-temperature water-gas shift reaction on Au/Fe_2O_3 and Au/TiO_2 catalysts, *J. Catal.* **188**(1), 176–185 (1999).
17. S. H. Overbury, L. Ortiz-Soto, H. G. Zhu, B. Lee, M. D. Amiridis, and S. Dai, Comparison of Au catalysts supported on mesoporous titania and silica: Investigation of Au particle size effects and metal-support interactions, *Catal. Lett.* **95**(3–4), 99–106 (2004).
18. A. Knell, P. Barnickel, A. Baiker, and A. Wokaun, Co Oxidation over Au/ZrO_2 catalysts—Activity, deactivation behavior, and reaction-mechanism, *J. Catal.* **137**(2), 306–321 (1992).
19. J. D. Grunwaldt, M. Maciejewski, O. S. Becker, P. Fabrizioli, and A. Baiker, Comparative study of Au/TiO_2 and Au/ZrO_2 catalysts for low-temperature CO oxidation, *J. Catal.* **186**(2), 458–469 (1999).
20. G. K. Bethke, and H. H. Kung, Selective CO oxidation in a hydrogen-rich stream over Au/gamma-Al_2O_3 catalysts, *Appl. Catal. A-Gen.* **194** 43–53 (2000).
21. G. C. Bond, and D. T. Thompson, Catalysis by gold, *Catal. Rev.-Sci. Eng.* **41**(3–4), 319–388 (1999).
22. G. C. Bond, and D. T. Thompson, Gold-catalysed oxidation of carbon monoxide, *Gold Bull.* **33**(2), 41–51 (2000).
23. A. Wolf, and F. Schuth, A systematic study of the synthesis conditions for the preparation of highly active gold catalysts, *Appl. Catal. A-Gen.* **226**(1–2), 1–13 (2002).

24. M. Haruta, Size- and support-dependency in the catalysis of gold, *Catal. Today* **36**(1), 153–166 (1997).
25. S. Schimpf, M. Lucas, C. Mohr, U. Rodemerck, A. Bruckner, J. Radnik, H. Hofmeister, and P. Claus, Supported gold nanoparticles: in-depth catalyst characterization and application in hydrogenation and oxidation reactions, *Catal. Today* **72**(1–2), 63–78 (2002).
26. A. Zwijnenburg, M. Saleh, M. Makkee, and J. A. Moulijn, Direct gas-phase epoxidation of propene over bimetallic Au catalysts, *Catal. Today* **72**(1–2), 59–62 (2002).
27. M. Haruta, Catalysis of gold nanoparticles deposited on metal oxides, *Cattech* **6**(3), 102–115 (2002).
28. T. V. Choudhary, and D. W. Goodman, Oxidation catalysis by supported gold nano-clusters, *Top. Catal.* **21**(1–3), 25–34 (2002).
29. G. Schmid, and B. Corain, Nanoparticulated gold: syntheses, structures, electronics, and reactivities, *Eur. J. Inorg. Chem.* (17), 3081–3098 (2003).
30. M. C. Daniel, and D. Astruc, Gold nanoparticles: Assembly, supramolecular chemistry, quantum-size-related properties, and applications toward biology, catalysis, and nanotechnology, *Chem. Rev.* **104**(1), 293–346 (2004).
31. W. F. Yan, and S. Dai, Primary- and secondary-support contributions to the activities of Au nanoparticles, to be submitted.
32. W. P. Huang, X. H. Tang, Y. Q. Wang, Y. Koltypin, and A. Gedanken, Selective synthesis of anatase and rutile via ultrasound irradiation, *Chem. Commun.* (15), 1415–1416 (2000).
33. Y. Q. Zheng, S. Erwei, S. X. Cui, W. J. Li, and X. F. Hu, Hydrothermal preparation and characterization of brookite-type TiO_2 nanocrystallites, *J. Mater. Sci. Lett.* **19**(16), 1445–1448 (2000).
34. S.-J. Lee, and A. Gavrilidis, Supported Au catalysts for low-temperature CO oxidation prepared by impregnation, *J. Catal.* **206,** 305–313 (2002).
35. D. Y. Zhao, Q. S. Huo, J. L. Feng, B. F. Chmelka, and G. D. Stucky, Nonionic triblock and star diblock copolymer and oligomeric surfactant syntheses of highly ordered, hydrothermally stable, mesoporous silica structures, *J. Am. Chem. Soc.* **120**(24), 6024–6036 (1998).
36. I. Ichinose, H. Senzu, and T. Kunitake, Stepwise adsorption of metal alkoxides on hydrolyzed surfaces: A surface sol-gel process, *Chem. Lett.* (10), 831–832 (1996).
37. G. Riegel, and J. R. Bolton, Photocatalytic efficiency variability in TiO_2 particles, *J. Phys. Chem.* **99**(12), 4215–4224 (1995).
38. E. Borgarello, J. Kiwi, E. Pelizzetti, M. Visca, and M. Gratzel, Sustained water cleavage by visible-light, *J. Am. Chem. Soc.* **103**(21), 6324–6329 (1981).
39. D. C. Hurum, A. G. Agrios, K. A. Gray, T. Rajh, and M. C. Thurnauer, Explaining the enhanced photocatalytic activity of Degussa P25 mixed-phase TiO_2 using EPR, *J. Phys. Chem.* B **107**(19), 4545–4549 (2003).
40. M. Haruta, B. S. Uphade, S. Tsubota, and A. Miyamoto, Selective oxidation of propylene over gold deposited on titanium-based oxides, *Res. Chem. Intermed.* **24**(3), 329–336 (1998).
41. K. Fukushima, G. H. Takaoka, J. Matsuo, and I. Yamada, Effects on CO oxidation activity of nano-scale Au islands and TiO_2 support prepared by the ionized cluster beam method, *Japan. J. Appl. Phys. Part 1—Regul. Pap. Short Notes Rev. Pap.* **36**(2), 813–818 (1997).
42. Y. Iizuka, T. Tode, T. Takao, K. Yatsu, T. Takeuchi, S. Tsubota, and M. Haruta, A kinetic and adsorption study of CO oxidation over unsupported fine gold powder and over gold supported on titanium dioxide, *J. Catal.* **187**(1), 50–58 (1999).
43. G. V. Samonsov, *The Oxide Handbook*, (IFI/Plenum, New York, 1982).
44. U. Diebold, The surface science of titanium dioxide, *Surf. Sci. Rep.* **48**(5–8), 53–230 (2003).
45. V. Schwartz, D. R. Mullins, W. F. Yan, B. Chen, S. Dai, and S. H. Overbury, XAS study of Au supported on TiO_2: influence of oxidation state and particle size on catalytic activity, *J. Phys. Chem.* B **108**(40), 15782–15790 (2004).
46. C. T. Campbell, Ultrathin metal films and particles on oxide surfaces: Structural, electronic and chemisorptive properties, *Surf. Sci. Rep.* **27**(1–3), 1–111 (1997).
47. I. Ichinose, H. Senzu, and T. Kunitake, A surface sol-gel process of TiO_2 and other metal oxide films with molecular precision, *Chem. Mater.* **9**(6), 1296–1298 (1997).

48. J. G. Huang, and T. Kunitake, Nano-precision replication of natural cellulosic substances by metal oxides, *J. Am. Chem. Soc.* **125**(39), 11834–11835 (2003).
49. J. H. He, I. Ichinose, T. Kunitake, A. Nakao, Y. Shiraishi, and N. Toshima, Facile fabrication of Ag-Pd bimetallic nanoparticles in ultrathin TiO2-gel films: Nanoparticle morphology and catalytic activity, *J. Am. Chem. Soc.* **125**(36), 11034–11040 (2003).
50. M. Leskela, and M. Ritala, Atomic layer deposition chemistry: Recent developments and future challenges, *Angew. Chem. Int. Ed.* **42**(45), 5548–5554 (2003).
51. T. Yasuda, R. Kuse, K. Iwamoto, K. Tominaga, and J. W. Park, Vapor-liquid hybrid deposition process for device-quality metal oxide film growth, *Chem. Mater.* **15**(22), 4157–4159 (2003).
52. J. W. Elam, D. Routkevitch, P. P. Mardilovich, and S. M. George, Conformal coating on ultrahigh-aspect-ratio nanopores of anodic alumina by atomic layer deposition, *Chem. Mater.* **15**(18), 3507–3517 (2003).